air concentrations of any two chemicals, implying the same basic transport mechanism for both of them, the fact that the relative concentrations do not remain constant with height shows that different vapor components approach zero concentration at different rates.

The relationship of the atmospheric profile to surface flux, particularly the energy elements momentum, sensible heat, and latent heat, is central in micrometeorology. One point of controversy is whether eddy dispersion is solely a property of atmospheric mixing and hence the same for all conservative entities (*9–11*). Resolution of this problem has often been hampered by instrumental errors and site-specific surface or atmospheric inhomogeneities. The fact that a different sensor is required to measure each energy property places severe demands upon instrument calibration and performance (*11, 12*). Measured profiles may be different because of systematic instrumental errors, unrecognized advected interferences, differences in the rates of eddy dispersion, or all three. Our experiment had no advected interferences, and all species were precisely measured in a single determination. Our data show that atmospheric dispersion rates are not the same for all conservative entities and also exhibit a clear reason why this is so.

The relative concentration changes among the pesticides always occurred in a definite order, and the pesticides may thus be ranked according to this order of profile depletion. This ranking is shown in Fig. 2 (*13*). According to the shape-function test of Swinbank and Dyer (*9*), profile depletion may be interpreted as a more rapidly increasing rate of eddy diffusion of the depleted component with height. The shape-function test thus reveals that eddy diffusivities increase more rapidly with height for components at the top of Fig. 2. The eddy diffusivities of the planar, aromatic herbicides trifluralin and Dacthal are greatest, and the eddy diffusivities tend to diminish as the degree of chlorination and the complexity of the ring structure increase. The ranking generally follows a pattern of increasing molecular weight (although lindane is an obvious exception), with further differences due to molecular shape, as suggested by the significant profile differences between the isomers dieldrin and photodieldrin.

The data show the effect of a single, continuous process in which vapors participate differently according to their molecular properties. Although the total transport rate is orders of magnitude greater, this predictable structuring of transport properties appears analogous to molecular diffusion. Because these pesticides have low vapor pressures, their vapor behavior is difficult to study in the laboratory and, as far as we know, measurements of their molecular diffusivity coefficients in air have not been reported. The actual molecular diffusivities are thus not known, but they would be expected to follow the ranking in Fig. 2, with the most rapidly diffusing components at the top.

We postulate that there exists a coupling of molecular diffusion and eddy dispersion into a single transport process in the free atmosphere, perhaps best described as an apparent acceleration of molecular diffusion as discussed by Monin and Yaglom (*14*). Therefore, differences in molecular weight and structure cannot be neglected when one is comparing the coefficients of dispersion of vapors in turbulent air.

D. E. GLOTFELTY
A. W. TAYLOR
Soil Nitrogen and Environmental Chemistry Laboratory, Agricultural Environmental Quality Institute, U.S. Department of Agriculture, Beltsville, Maryland 20705
W. H. ZOLLER
Chemistry Department, University of Maryland, College Park 20742

References and Notes

1. O. G. Sutton, *Micrometeorology* (McGraw-Hill, New York, 1953).
2. D. E. Glotfelty, thesis, University of Maryland (1981).
3. The compounds, molecular weights, and vapor pressures (in millimeters of mercury) at 25°C are as follows: trifluralin, 335, 1.1×10^{-4}; Dacthal, 332, 2.5×10^{-6}; heptachlor, 373, 3×10^{-4}; chlordane, 410, 1×10^{-5}; lindane, 291, 6.3×10^{-5}; dieldrin, 381, 5.4×10^{-6}; and photodieldrin, 381, unknown. Field data on dieldrin and photodieldrin were obtained in earlier studies (*4, 5*).
4. A. W. Taylor, D. E. Glotfelty, B. L. Glass, H. P. Freeman, W. M. Edwards, *J. Agric. Food Chem.* **24**, 625 (1976).
5. A. W. Taylor, D. E. Glotfelty, B. C. Turner, R. E. Silver, H. P. Freeman, A. Weiss, *ibid.* **25**, 542 (1977); B. C. Turner, D. E. Glotfelty, A. W. Taylor, *ibid.*, p. 548.
6. B. C. Turner and D. E. Glotfelty, *Anal. Chem.* **49**, 7 (1977).
7. L. H. Parmele, E. R. Lemon, A. W. Taylor, *Water Air Soil Pollut.* **1**, 433 (1972).
8. E. Atlas and C. S. Giam, *Science* **211**, 163 (1981).
9. W. C. Swinbank and A. J. Dyer, *Q. J. R. Meteorol. Soc.* **93**, 494 (1967).
10. A. J. Dyer and B. B. Hicks, *ibid.* **96**, 715 (1970); J. A. Businger, J. C. Wyngard, Y. Izumi, E. F. Bradley, *J. Atmos. Sci.* **28**, 181 (1971); W. O. Pruitt, D. L. Morgan, F. J. Lourence, *Q. J. R. Meteorol. Soc.* **99**, 370 (1973); A. J. Dyer, *Boundary-Layer Meteorol.* **7**, 363 (1974); B. B. Hicks, *Q. J. R. Meteorol. Soc.* **102**, 535 (1976).
11. A. M. Yaglom, *Boundary-Layer Meteorol.* **11**, 89 (1977).
12. J. Wieringa, *ibid.* **18**, 411 (1980).
13. Dacthal was ranked for periods when particulate Dacthal was absent. Data for dieldrin and photodieldrin were from (*4, 5*). Chlordane and dieldrin were not directly compared in field studies; we judged their positions by comparing each to heptachlor.
14. A. S. Monin and A. M. Yaglom, *Statistical Fluid Mechanics: Mechanics of Turbulence* (MIT Press, Cambridge, Mass., 1971), pp. 591–606.

12 October 1982

Attogram Detection Limit for Aqueous Dye Samples by Laser-Induced Fluorescence

Abstract. *A modified flow cytometer has been used to detect attogram quantities of aqueous rhodamine 6G by laser-induced fluorescence analysis. A detection limit of 28 attograms (35,000 molecules) was obtained, nearly two orders of magnitude better than earlier measurements. The detection limit in concentration units was* 1.4×10^{-13} *mole per liter. During the 1-second measurement period, the total volume sampled was 0.42 microliter. On average, only half a rhodamine 6G molecule was present in the 6-picoliter probed volume.*

Laser-induced fluorescence analysis of liquid samples is of broad interest because of the exceedingly low detection limits attainable with the technique. Applications range from fluoroimmunoassay (*1*) to the detection of liquid chromatographic eluents (*2*). It is desirable to decrease the detection limits of the technique to allow analysis of smaller samples, minimize detector volume in high-performance liquid chromatography, and reduce the number of fluorescent tags needed in fluoroimmunoassay (*3*). We present here a straightforward method for the detection of attogram amounts (1 ag = 10^{-18} g) of aqueous dye based on the use of laser-induced fluorescence with an instrument designed for flow cytometry (*4*). More details of this work and a comparison of several flow cytometer experimental arrangements for fluorescence detection are presented in (*5*).

The hydrodynamic focusing technique used in flow cytometry provides a well-designed flow chamber that has been used for the analysis of small samples with laser-induced fluorescence (*6, 7*). By using a slow sample flow rate, one can analyze submicroliter volumes. Probed volumes in a flow cytometer can be as small as a few picoliters (1 pl = 10^{-12} liter). The optical arrangement of the flow cytometer provides an improved signal-to-noise ratio in comparison with conventional flow cells by

Table 1. Comparison of laser-induced fluorescence detection limits.

Reference	Sample	Solvent	Light source	Probed volume*	Sampled volume† (μl)	Flow rate (ml/min)	Time constant (seconds)	Detection limit‡	
								Grams	Molecules
This work	Rhodamine 6G	Water	250 mW, 514.5 nm	6 pl	~ 0.42	0.025	~ 1	2.8×10^{-17}	3.5×10^{4}
(*8*)	Fluoranthene	Hexane	1.5 W, 351 nm	1 nl	~ 17	2	~ 0.5	6.0×10^{-16}	1.8×10^{6}
(*6*)	Rhodamine 6G	Water	8 mW, 488 nm	3.8 nl	~ 25	1	~ 1.7	5.3×10^{-15}	7×10^{6}
(*9*)	Aflatoxin	Water:methanol (3:1)	8 mW, 325 nm	4 μl	~ 75	1.5	~ 3	2.6×10^{-14}	5×10^{7}

*Volume of the intersection of the laser beam and sample stream. †Volume that flows through the detector in one time constant. ‡For chromatographic data, the peak concentration is calculated as in (*9*). A concentration detection limit is computed for a signal-to-noise ratio of 2 and a 1-second time constant. The mass concentration limit is then defined as the product of the concentration detection limit, in grams per liter, multiplied by the volume flow rate, in liters per second, multiplied by 1 second.

minimizing the collection of light scattered from the chamber windows.

The flow cytometer used in this work was a modified Becton-Dickinson FACS II cell sorter (Fig. 1). The flow system was modified to use a flow cuvette obtained from an Ortho Instruments System 50 flow cytometer. This flow cell produces relatively little scattered light. The square bore of the cuvette is 0.25 mm on a side. The sample flow rate was 25 μl/min, and the stream diameter was 20 μm.

Fresh solutions of aqueous rhodamine 6G were prepared within 48 hours of the measurements from a $3.5 \times 10^{-7}M$ stock solution by serial dilution in filtered, deionized water of low organic content. This treated water was also used as the sheath fluid. Background measurements were obtained with the sample stream off and only sheath fluid flowing.

An argon-ion laser (Spectra-Physics, model 165-05) was used at 514.5 nm in the light-regulated mode. An electro-optic modulator (Coherent, model 50) was used to chop the laser beam at 10 kHz in a square wave with 50 percent duty cycle. The laser beam was focused with a lens (5-cm focal length) to a waist 10 μm in radius (e^{-2} in intensity) at the sample stream. The average laser power delivered to the sample was 0.25 W. No optical saturation effects were noted.

A microscope objective, 32× and numerical aperture = 0.6 (10 percent collection efficiency), imaged the illuminated region onto a pinhole 0.75 mm in diameter to decrease the collection of light scattered from regions outside the probed volume. The fluorescence light was then passed through three spectral filters to reduce scattered laser light: a bandpass interference filter centered at 550 nm with 40-nm full width at half-maximum, a longwave pass interference filter with 50 percent cut-on at 530 nm, and a longwave pass colored-glass filter with 50 percent cut-on at 530 nm (Shott type OG530). An S20 photomultiplier (EMI 9798A), selected for low noise and high photocathode sensitivity, was operated at 600 V to detect the light.

The photomultiplier signal was preamplified and sent to a lock-in amplifier (Princeton Applied Research, model 124), phase-referenced to the electro-optic modulator. The lock-in output was integrated for 1.0 second with a voltage-to-frequency converter (Analog Devices A60L) and a pulse counter (Hewlett-Packard, model 5214L). A sequence of five to ten readings was recorded, and the mean and standard deviation were calculated.

Laser-induced fluorescence was measured for aqueous rhodamine 6G solutions ranging in concentration from $3.5 \times 10^{-11}M$ to $3.5 \times 10^{-8}M$. The resulting calibration curve is linear, correlation coefficient (R) > .999, across the concentration range studied. The detection limit, 2 standard deviations above background, in mass units is 28 ag and in concentration units is $1.4 \times 10^{-13}M$. This limit corresponds to 35,000 molecules flowing through the probed volume during the 1-second integration time. On the average, only half a dye molecule is present within the probed volume at the detection limit. The results of this experiment are compared with other laser-induced fluorescence experiments for flowing samples in Table 1 (*6, 8, 9*). Our results are nearly two orders of magnitude better than earlier measurements. This improvement arises from the use of a very small detection volume, a modulated laser beam with phase-sensitive detection electronics, and careful spatial and spectral filtering of scattered light.

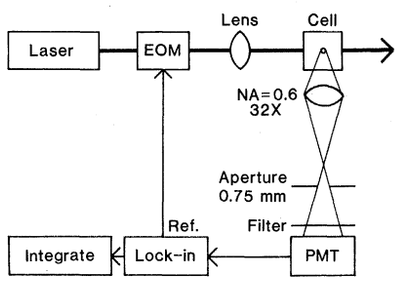

Fig. 1. Experimental diagram. An argon-ion laser beam, wavelength = 514.5 nm, is chopped with an electro-optic modulator (*EOM*) at 10 kHz. A lens (5-cm focal length) focuses the laser light into the flow cytometer cuvette (*Cell*). Fluorescence is collected at right angles by a microscope objective (32×; numerical aperture = 0.6). A 0.75-mm aperture is placed in the focal plane to restrict the detector's field of view to the probed volume. Spectral filters are used to reduce scattered laser light which reaches the photomultiplier tube (*PMT*). The output of the photomultiplier tube is preamplified and sent to a lock-in amplifier phase-referenced to the electro-optic modulator. The lock-in amplifier analog output is integrated for 1-second intervals with an analog-to-digital converter.

In biological studies of the cell surface, it is becoming increasingly important to detect small numbers of binding sites. For example, the importance of measuring small numbers of insulin receptor sites in diabetes research has recently been emphasized (*10*). Our results may be used to estimate the minimum number of binding sites with a fluorescent tag needed to discriminate between labeled and unlabeled biological cells in conventional flow cytometry. At a linear flow velocity of 1 m/sec, the cell transit time through the laser beam is 20 μsec. If we assume a square-root dependence of the signal-to-noise ratio upon integration time, the calculated detection limit in 20 μsec is 160 molecules. Measurements of this type will require use of a d-c laser beam coupled with photon counting techniques. Preliminary measurements with pulsed data acquisition have yielded essentially the same detection limits. This number is a lower bound on the number of fluorescent tags needed to discriminate between labeled and unlabeled cells. Autofluorescence of the cell, fluorescence quenching, and increased background scatter from cells act to degrade this detection limit.

Possible improvements in system performance could be obtained with a lower sample flow rate, higher laser power, improved fluorescence collection effi-

ciency, optimized spectral filtering, higher photomultiplier quantum yield, and electronic correlation filtering (*11*) matched to the transit time of a molecule through the laser beam. On the basis of reasonable estimates for signal-to-noise improvements, it may be possible to detect a single molecule passing through the probed volume (*5*). This would be a significant improvement in laser-induced fluorescence detection limits. Single-molecule detection limits also provide the ultimate in sample quantitation wherein uncertainties are dominated by counting statistics in the number of molecules processed.

NORMAN J. DOVICHI*
JOHN C. MARTIN
JAMES H. JETT
RICHARD A. KELLER
Los Alamos National Laboratory, Los Alamos, New Mexico 87545

References and Notes

1. D. S. Smith, M. Hassan, R. D. Nargessi, in *Modern Fluorescence Spectroscopy*, E. L. Wehry, Ed. (Plenum, New York, 1981), vol. 3, p. 143.
2. E. S. Yeung and M. J. Sepaniak, *Anal. Chem.* **52**, 1465A (1980).
3. T. Hirschfeld, *Appl. Opt.* **15**, 3135 (1976).
4. M. R. Melamed, P. F. Mullaney, M. L. Mendelsohn, *Flow Cytometry and Sorting* (Wiley, New York, 1979).
5. N. J. Dovichi, J. C. Martin, J. H. Jett, R. A. Keller, in preparation.
6. T. A. Kelly and G. D. Christian, *Anal. Chem.* **53**, 2110 (1981).
7. L. W. Hershberger, J. B. Callis, G. D. Christian, *ibid.* **51**, 1444 (1979).
8. S. Folestad, L. Johnson, B. Josefsson, B. Galle, *ibid.* **54**, 925 (1982).
9. G. J. Diebold and R. N. Zare, *Science* **196**, 1439 (1977).
10. T. J. Robinson, J. A. Archer, K. K. Gambhir, V. W. Hollis, Jr., L. Carter, C. Bradley, *ibid.* **205**, 200 (1979).
11. B. Reiffen and H. Sherman, *Proc. IEEE* **51**, 1316 (1963).
12. We thank D. M. Holm for his advice and encouragement. This work was supported by the Department of Energy.
* Present address: Department of Chemistry, University of Wyoming, Laramie 82071.

12 October 1982

Dynamical Consequences of Orthohydrogen-Parahydrogen Disequilibrium on Jupiter and Saturn

Abstract. *The Voyager observation of high zonal flow speeds (about 400 meters per second) in the atmosphere of Saturn has raised fundamental questions about the flow on both Jupiter and Saturn. One possibility is that the flow is extremely deep, perhaps extending through the planet. Another is that the flow is confined near the cloud tops and is associated with very strong buoyancy contrasts. It is demonstrated that the heat of conversion from parahydrogen to orthohydrogen can provide buoyancy contrasts of the required magnitude, and a feedback mechanism is proposed to couple the heat of conversion to the flow dynamics.*

Jupiter and Saturn have internal heat sources whose strengths have been well determined by Voyager spacecraft measurements (*1, 2*). In both cases the energy release is large enough that the interiors should be convective but small enough that, according to conventional theories of convection, the temperature (T) fluctuations are extremely small (*3*), with the fractional change $\delta T/T \sim 10^{-6}$. The simplest conventional treatment of convection is the mixing length theory presented in stellar structure textbooks (*4*), and its most severe test is in application to the sun. There it successfully predicts the observed length scale and time scale of the photospheric granulation (to an order of magnitude, which is all it attempts).

But the simplest ideas fail on Jupiter and Saturn. First, the strong long-lived mean zonal flows detected by the Voyager experiments (*5, 6*) are strikingly at variance with the small-scale turbulence that would be expected. Second, and more quantitatively, it can be inferred from the observed velocities that the temperature fluctuations associated with motions are much larger than theory predicts (unless there is a special geometry to the flow field; see point 3 below). In light of this discrepancy it is important to examine the thermodynamics of the mixtures that compose these atmospheres and to reach an understanding of how they differ from the simple fluids assumed in ordinary convection theory. Those fluids are in local thermodynamic equilibrium, composed of a single constituent, and buoyancy is therefore proportional to heat content. In this report we show that lack of thermodynamic equilibrium between orthohydrogen and parahydrogen in the outer planets can lead to buoyancy effects in their atmospheres that may be large enough to explain the observations. Massie and Hunten (*7*) recently examined equilibration rates and found that they are slow, of the same order as the expected dynamical time scales, although exact rates remain an important uncertainty.

There are, of course, other differences between Jupiter or Saturn and the sun. A key one is the latitudinal distribution on the planets of external heating due to insolation, which energetically is the same order of magnitude as the internal heat. The geometry of the flow may be determined by this boundary condition while the amplitude of buoyancy contrasts is determined by the thermodynamics; we focus in this report on the latter.

How do the observations indicate large temperature fluctuations on Jupiter and Saturn? Steady atmospheric flows on rotating planets are associated with horizontal pressure gradients. In a fluid planet these pressure gradients cannot be produced mechanically by simple accumulation of excess atmospheric mass over certain locations, since there is no rigid surface to support the weight. Instead, there must be horizontal temperature contrasts to puff up different atmospheric columns by different amounts so that, for example, if there is no horizontal pressure gradient between the bases of two columns then one will exist between the tops. Specifically, the change of zonal wind u with height is related to the latitudinal temperature gradient $\partial T/\partial y$ by (*8*)

$$u(p_1) - u(p_2) = \frac{R}{f}\int_{p_1}^{p_2}\frac{\partial T}{\partial y}\frac{dp}{p} \qquad (1)$$

where p_1 and p_2 are the atmospheric pressures at two different levels, R is the gas constant, f is the Coriolis parameter, and the temperature gradient is evaluated along a surface of constant pressure. Assume that the observed dynamical regime is confined to a depth of N pressure scale heights (e-foldings of pressure) below the observed clouds. Then Eq. 1 tells us that to an order of magnitude

$$\delta T \sim \frac{fL}{NR}U \qquad (2)$$

where L is the observed horizontal scale of wind variation and U is the wind speed. This is the relationship that provides an estimate of temperature contrasts. In the following discussion we will adopt for both planets $f = 1.76 \times 10^{-4}$ sec^{-1} (corresponding to about 30° latitude), $L = 2000$ km (corresponding to a latitudinal wavelength of the zonal flow oscillation of about 13,000 km), and $R = 4.16$ J g^{-1} K^{-1} (corresponding to hydrogen). These values are sufficiently accurate for the arguments presented below, and a single set of parameters for both planets will help later to display clearly the changes between the two in hydrogen disequilibrium.

The following points are important.

1) As the Voyager imaging team pointed out (*6*), the high flow speeds on Sat-